# ARTICLES

## Applications of a tight-binding total-energy method for transition and noble metals: Elastic constants, vacancies, and surfaces of monatomic metals

Michael J. Mehl and Dimitrios A. Papaconstantopoulos

*Complex Systems Theory Branch, Naval Research Laboratory, Washington, D.C. 20375-5345*

A recent tight-binding scheme provides a method for extending the results of first-principles calculations to regimes involving $10^2 - 10^3$ atoms in a unit cell. The method uses an analytic set of two-center, nonorthogonal tight-binding parameters, on-site terms that change with the local environment, and no pair potential. The free parameters in this method are chosen to simultaneously fit band structures and total energies from a set of first-principles calculations for monatomic fcc and bcc crystals. To check the accuracy of this method we evaluate structural energy differences, elastic constants, vacancy formation energies, and surface energies, comparing to first-principles calculations and experiment. In most cases there is good agreement between this theory and experiment. We present a detailed account of the method, a complete set of tight-binding parameters, and results for 29 of the alkaline-earth, transition, and noble metals. [S0163-1829(96)01931-5]

## I. INTRODUCTION

Recently, a total-energy tight-binding (TB) method was introduced[1] wherein the parameters were fit to the total energies and band structures obtained from a limited set of first-principles calculations. The method produces very good structural energy differences, elastic constants, phonon frequencies, vacancy formation energies, and surface energies for the transition and noble metals. In this paper we thoroughly examine the method for these elements and for the alkaline-earth metals.

Section II describes the method, including the analytic expressions for the tight-binding parameters and the scheme for fitting them to first-principles theory. The remainder of the paper discusses the predictions made by this method. Section III shows that the method correctly predicts the ordering of several metallic phases, including the 29-atom $\alpha$Mn phase, and correctly predicts the energy differences between the lower phases. Section IV discusses the calculation of elastic constants. Since these calculations can also be performed by first-principles techniques,[2–5] we compare our TB results with those obtained from first-principles to assess the accuracy of the method. We can also use the method to study systems that have relatively large (20–200 atom) unit cells, a regime that requires laborious first-principles calculations, but which can be done very quickly by our TB method. In Sec. V we discuss the structure and energetics of vacancies and in Sec. VI we consider surface energetics. Finally, in Sec. VII we summarize our results, discuss possible methods to improve our agreement with first-principles theory or experiment, and consider the course of future improvements to the method.

## II. TIGHT-BINDING METHOD

Density-functional theory (DFT),[6] using the Kohn-Sham ansatz for the kinetic energy,[7] tells us that the total energy of a system of electrons moving in a solid can be written in the form

$$E[n(\mathbf{r})] = \sum_i f(\mu - \varepsilon_i)\varepsilon_i + F[n(\mathbf{r})], \qquad (1)$$

where $n(\mathbf{r})$ is the electronic density, $\varepsilon_i$ is the Kohn-Sham eigenvalue of the $i$th electronic state, $\mu$ is the chemical potential, and the sum is over all electronic states of the system. Since we will be primarily interested in studying metals, we take the function $f(\mu - \varepsilon)$ to have the Fermi function form[8]

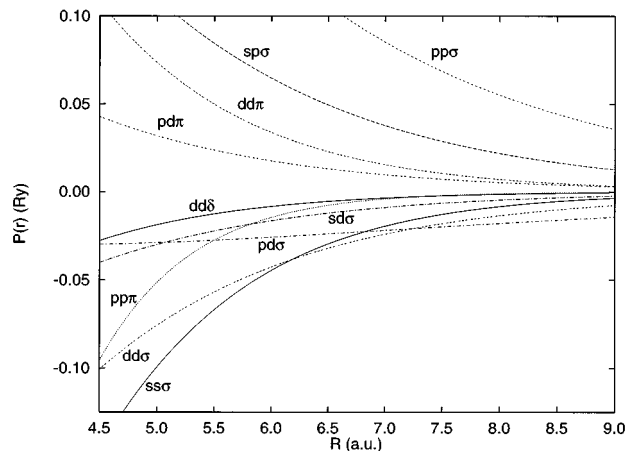$$f(z) = \frac{1}{1 + e^{\beta z}}, \qquad (2)$$



FIG. 1. Values of the two-center Slater-Koster integrals for the Hamiltonian matrix as a function of distance for molybdenum, obtained from the tight-binding parameters (10). The integrals are labeled according to the standard notation (Refs. 17 and 19).

<u>54</u>          4519

where $\beta = 1/kT$. Typically we take $T$ between 2 and 5 mRy. The functional $F[n(\mathbf{r})]$ contains the remaining part of the DFT total energy: the ion-ion interaction energy, the parts of the Hartree and exchange-correlation energy not included in the eigenvalue sums, and corrections for double counting in the eigenvalue sums.

Many tight-binding methods use (1) to provide a natural separation between the parts of $E[n(\mathbf{r})]$ that can be treated by tight binding and the parts that must be treated by other means.[9–16] In these cases the eigenvalue sum is calculated by tight-binding methods and $F[n(\mathbf{r})]$ is approximated by a sum of pair potentials.

We have developed an alternative method of applying tight binding to (1),[1] based on the fact that the Kohn-Sham method allows an arbitrary shift in the potential. If this shift is defined to be

$$V_0 = F[n(\mathbf{r})]/N_e , \qquad (3)$$

where

$$N_e = \sum_i f(\mu - \varepsilon_i) \qquad (4)$$

is the number of electrons in the system, then the eigenvalues $\varepsilon_i$ are each shifted by an amount $V_0$, to the new values

$$\varepsilon_i' = \varepsilon_i + V_0 . \qquad (5)$$

The total energy (1) then becomes

$$E[n(\mathbf{r})] = \sum_i f(\mu' - \varepsilon_i')\varepsilon_i' , \qquad (6)$$

where $\mu' = \mu + V_0$ is the shifted chemical potential.

By the density-functional theorem,[6] the shifted eigenvalues $\varepsilon_i'$ can be considered to be functions of the crystal structure, including volume, primitive lattice vectors, and internal parameters. A tight-binding method that reproduces the $\varepsilon_i'$ over a range of structures will then solve the total-energy problem (1) or (6) without resort to an additional term.

The two-center Slater-Koster formulation[17] of tight binding with a nonorthogonal basis breaks the problem into the calculation of three types of parameters: on-site parameters, which represent the energy required to place an electron in a specific orbital; Hamiltonian parameters, which represent the matrix elements for electrons hopping from one site to another; and overlap parameters, which describe the mixing between the nonorthogonal orbitals on neighbor sites. The eigenvalues $\varepsilon_i'$ can be determined once the parameters are evaluated for a given structure. The basic method we use is to give the Slater-Koster parameters simple algebraic forms, with parameters chosen to reproduce first-principles results over a wide range of structures.

In an orthogonal tight-binding calculation, applying the shift (5) to each eigenvalue would be equivalent to shifting each diagonal element of the Hamiltonian matrix by an amount $V_0$. In the nonorthogonal case the effect is slightly more complicated. It is clear, however, that the Hamiltonian and overlap parameters should not directly depend on the shift $V_0$. Thus the effect of (5) can only be accounted for by changing the on-site parameters. These parameters must now be sensitive to the local environment around each atom. We

describe this local environment by introducing a ''density'' associated with each atom, defined by

$$\rho_i = \sum_{j \neq i} \exp[-\lambda_{\tilde{j}\tilde{\imath}}^1 R_{ij}] F_c(R_{ij}), \qquad (7)$$

where $\tilde{\imath}(\tilde{\jmath})$ denotes the type of atom on site $i$ ($j$), $\lambda$ is a parameter that will depend on the atom types, $R_{ij}$ is the distance between atoms $i$ and $j$, and $F_c(R)$ is a smooth cutoff function

$$F_c(R) = \{1 + \exp[(R - R_0)/l]\}^{-1}, \qquad (8)$$

which we use to limit the range of the parameters. In the calculations shown here we typically take $R_0 = 14.0a_0$ and $l = 0.5a_0$ (where $a_0$ denotes the Bohr radius), which effectively zeros all interactions for neighbors more than $16.5a_0$ apart. Depending on the structure and lattice constant, this radius will include 80 – 300 neighboring atoms.

Although, in principle, the on-site terms should have off-diagonal elements due to the overlap of the on-site wave functions with neighboring atomic potentials,[18] we follow traditional practice and only include the diagonal terms, keeping only the terms corresponding to $s$, $p$, and $d$ orbitals. The on-site term for atom $i$ is

$$h_{i\alpha} = a_{\tilde{\imath}\alpha} + b_{\tilde{\imath}\alpha}\rho_i^{2/3} + c_{\tilde{\imath}\alpha}\rho_i^{4/3} + d_{\tilde{\imath}\alpha}\rho^2, \qquad (9)$$

where $\alpha = s$, $p$, or $d$ and $\rho_i$ is given by (7). To show the correspondence between this theory and previous theories, note that $\rho$ in (7) has a form similar to a pair potential. Thus, if (9) were linear in $\rho$, we restricted ourselves to an orthogonal Hamiltonian, and kept $h_{i\alpha}$ independent of the angular momentum, then (9) would just be a method of parametrizing $F[n(\mathbf{r})]$ by a simple pair potential. Seen in this light, the density-dependent parts of the on-site term (9) can be regarded as a generalized pair potential.

In general, the Hamiltonian and overlap Slater-Koster parameters may depend upon the structure and local environment of the atoms, even in the case of the two-center approximation. This approach, while valid, will lead to many complications when we extend the method to include other crystal structures and binary alloys. We therefore constrain the form of these parameters so that they depend only on the distance between the two atoms. Both the Hamiltonian and overlap parameters are assumed to have the same functional form

$$P_\gamma(R) = (e_\gamma + f_\gamma R)\exp[-g_\gamma^2 R] F_c(R), \qquad (10)$$

where $\gamma$ indicates the type of interaction (e.g., $ss\sigma$, $pd\pi$, etc.), $R$ is the distance between the atoms, and $F_c(R)$ is given by (8).

In the monatomic case, restricting ourselves to $s$, $p$, and $d$ orbitals, there are three on-site Slater-Koster parameters (9), with 13 parameters required to completely specify them. Similarly, there are 10 Hamiltonian and 10 overlap parameters (10), each requiring 3 parameters. Thus, to completely specify the Slater-Koster tight-binding scheme in this model requires the determination of at most 73 parameters. In practice, we only used the $d_{\tilde{\imath}\alpha}$ found in (9) in the parametrization of Ti, Zr, and Hf, so for most elements we had only 70 independent parameters. The parameters are determined by
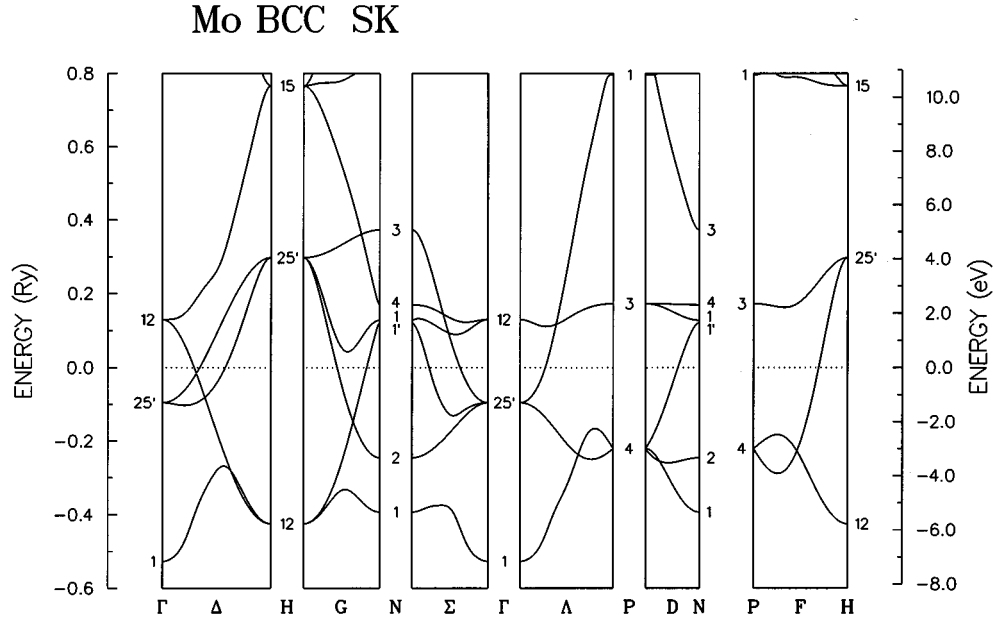
## Mo BCC SK



FIG. 2. Tight-binding electronic band structure of bcc Mo at the LDA equilibrium lattice constant (3.12 Å). The energies of the eigenstates have been uniformly shifted to set the Fermi level to zero.

requiring that the eigenvalues determined by the Slater-Koster parameters[19] [(7)–(10)] reproduce the electronic band structure [including the eigenvalue shift (3)] produced by a set of first-principles density-functional calculations and that the corresponding energies (6) reproduce the first-principles energies. For the metals discussed here we use either the muffin-tin potential augmented plane wave[20] (APW) or the full-potential linearized augmented plane wave[21,22] (LAPW) method to calculate the electronic band structure and total energies for 4–6 volumes in each of the fcc and bcc structures, using uniform $k$-point meshes that include the origin and contain 89 and 55 points, respectively. In all cases we used the Hedin-Lundqvist parametrization[23] of the local-density approximation[7] (LDA) to DFT. Possible spin polarization is ignored. For a typical transition metal there are about 4000 eigenvalues and energies in the database. We use an IMSL package, based on a finite-difference Levenberg-Marquardt algorithm,[24] to adjust the 70 (or 73) parameters to reproduce this database by means of a nonlinear least-squares fit, with the total energies typically weighted about 200 times larger than the eigenvalues in a single band. We place additional conditions on the minimization as follows. Since the overlap matrix defined by the parameters (10) must, physically, be positive definite, a function that penalizes small or negative determinant overlap matrices is included. While this does not guarantee that our overlap matrix will remain positive definite during the minimization process, it does tend to keep the determinant from changing sign, meaning that an overlap matrix that is originally positive definite tends to stay that way. We also restrict the behavior of the functions (10). Physically, we expect both the Hamiltonian and overlap parameters to decay steadily and not change sign for distances $R$ near or greater than the nearest-neighbor distance. We thus add another contribution to our minimization function, which penalizes parameter sets $(e_\gamma, f_\gamma, g_\gamma)$ that cause either $P_\gamma(r)$ or $P'_\gamma(r)$ to vanish over

the range of distances where we are likely to require evaluation of the Slater-Koster matrix elements. Finally, we select our starting parameters guided by those found in previous work[19] and ensure that the symmetry of the eigenstates is taken into account.

As an illustration of the above technique, we present several results for molybdenum. Using the APW program, we calculated the total energy and band structure of Mo at four volumes in the fcc structure and five volumes in the bcc structure. The parameters in (7), (9), and (10) were then adjusted to best fit the total energies and the band structure in the lower six bands of Mo over all nine volumes. The resulting two center Slater-Koster parameters (10) are shown in Fig. 1 for the Hamiltonian matrix elements. We note that there is a smooth and monotonic decay of the TB parameters towards zero. To assess the quality of the fit, we calculate the tight-binding band structure of Mo at the LDA equilibrium volume (3.12 Å) of the bcc structure (Fig. 2) and compare it to the first-principles band structure (Fig. 3).[19] We see that the band structures are in close agreement over the entire Brillouin zone and a wide spectrum of energies, with some deterioration far above the Fermi level. We also calculate the energy-volume behavior for a large number of phases and compare the fcc and bcc energies to those obtained from APW calculations, as shown in Fig. 4. We see that there is excellent agreement between the tight-binding and first-principles curves for the fcc and bcc structures and that all other structures, including hcp, are above the bcc ground state.

The above procedure works well for all of the metals described here except vanadium, where the elastic constant $C_{44}$ is predicted to be 172 GPa, compared to 30 GPa found experimentally[25] and 43 GPa when found using the first-principles LAPW method. This discrepancy is probably due to the high electronic density of states in vanadium near the Fermi level.[19] To better describe the electronic structure of
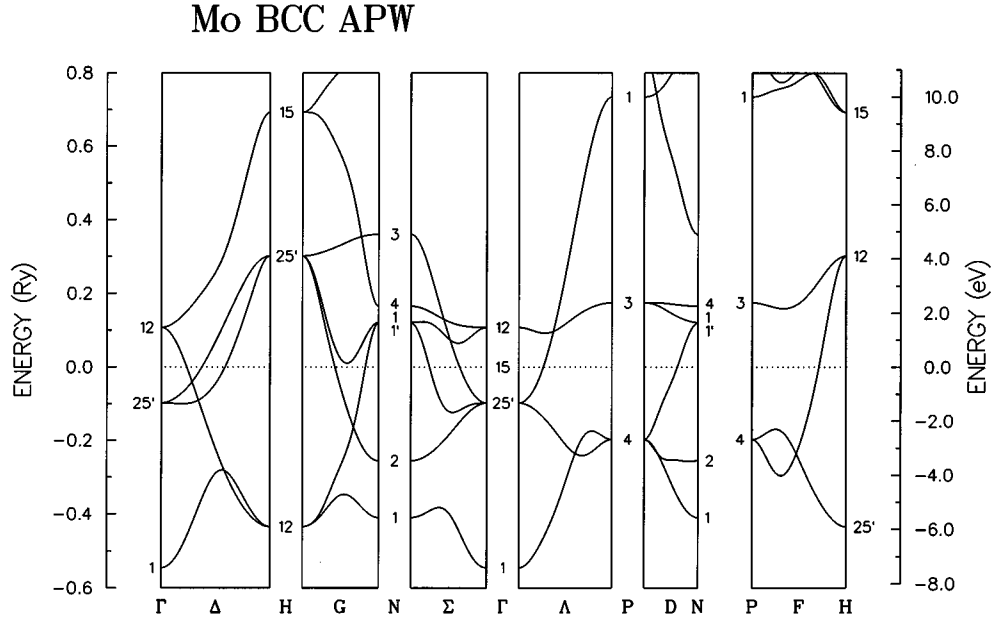
## Mo BCC APW

FIG. 3. Self-consistent first-principles LDA electronic band structure of bcc Mo at the LDA equilibrium lattice constant (3.12 Å), as determined by the muffin-tin APW program (Ref. 20). The energies of the eigenstates have been uniformly shifted to set the Fermi level to zero.

vanadium we have made two changes to the above formalism. First, we split the $d$ on-site energy (9) into contributions from the $t2g$ and $eg$ levels.[19] Second, we increase our parameter space by modifying the Slater-Koster parameter's functional form (10) to include a quadratic term

$$P_\gamma(R)=(e_\gamma+f_\gamma R+\overline{f}_\gamma R^2)\exp[-g_\gamma^2 R]F_c(R). \quad (11)$$

This procedure adds an additional 24 parameters to our basis set, for a total of 97. We reduce this by setting $d_\alpha=0$ in (9) for $\alpha=s$, $p$, $t2g$, and $eg$. When we fit the remaining 93

FIG. 4. Energy-volume behavior of molybdenum in several phases, using the tight-binding method. The energy of the diamond structure is not shown, as its minimum energy is 0.116 Ry above the origin. The small symbols ( ◇ ) represent the APW energies of the bcc and fcc phases. The construction of the $L1_2$ and $D0_3$ lattices is discussed in Table II. The origin of the energy was chosen arbitrarily.

parameters, as above, we reduce the predicted elastic constant $C_{44}$ to 92 GPa without significantly changing our other predictions. While this is not in perfect agreement with experiment, it is a substantial improvement, so we will use these parameters for vanadium in preference to the 73 parameter set, which gives a worse elastic constant.

We have used this method to determine tight-binding parameters for most of the alkaline-earth, transition, and noble metals. In the case of the antiferromagnetic (Cr and Mn) and magnetic (Fe, Co, and Ni) elements we restricted our calculations to the nonmagnetic case. This causes some difficulty when comparing our results to experiment, as shown below. The parameters for La are not presented because its $f$ bands are located in the middle of the $d$ bands[19] and therefore it is impossible to fit within our formalism. The Appendix lists various methods of obtaining the parameters used in this paper.

### III. GROUND-STATE BEHAVIOR AND PHASE STABILITY

We first test our parameter sets by looking at the equation of state for the observed ground state of each element. For the fcc and bcc nonmagnetic cubic crystals, our parameters should reproduce the first-principles results for these phases because of the fitting procedure. For the hcp elements and manganese, these calculations serve as a tight-binding prediction of the equation of state. The case of manganese has been discussed in more detail elsewhere.[26]

Table I shows the equilibrium lattice constants and bulk moduli for all of the metals studied here, comparing them to first-principles LAPW calculations,[3,5] muffin-tin APW calculations,[20] and to experiment.[27,28] For the nonmagnetic cubic crystals, the equilibrium lattice constant is within 1% of the first-principles LDA value for all of the cubic elements
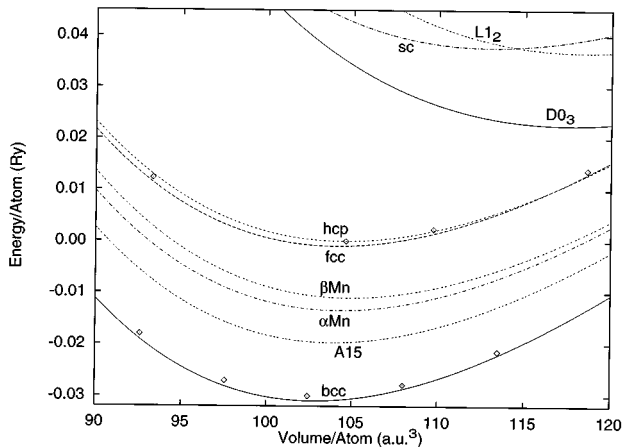
TABLE I. Equilibrium lattice constants and bulk moduli for the experimentally observed ground-state structures of the elements, comparing the results of our tight-binding parametrization (TB), first-principles local density approximation (LDA) results, where available, and experiment (Expt.) (Refs. 27 and 28). Where not referenced, the LAPW results were done for this paper, using previously developed methods (Ref. 4).

| Element | Structure | $a$ (Å) | | | $c$ (Å) | | | $B_0$ (GPa) | | |
|---|---|---|---|---|---|---|---|---|---|---|
| | | TB | LDA | Expt. | TB | LDA | Expt. | TB | LDA | Expt. |
| Ca | fcc | 5.30 | 5.34[a] | 5.58 | $a$ | $a$ | $a$ | 21 | 19 [a] | 15 |
| Sc | hcp | 3.26 | 3.21[b] | 3.31 | 4.91 | 5.01 [b] | 5.27 | 63 | 65 [b] | 44 |
| Ti | hcp | 2.97 | 2.87 | 2.95 | 4.80 | 4.55 | | 4.68 | 122 | 120 | 105 |
| V | bcc | 2.94 | 2.93 | 3.03 | $a$ | $a$ | $a$ | 211 | 196 | 162 |
| Cr | bcc | 2.80[c] | | 2.88 | $a$ | | $a$ | 283 | | 190 |
| Mn | $\alpha$Mn | 8.41[c] | | 8.91 | $a$ | | $a$ | 320 | | 60 |
| Fe | bcc | 2.71[c] | | 2.87 | $a$ | | $a$ | 281 | | 168 |
| Co | hcp | 2.40[c] | | 2.51 | 3.90 [c] | | 4.07 | 384 | | 191 |
| Ni | fcc | 3.43[c] | 3.42[d] | 3.52 | $a$ | $a$ | $a$ | 268 | 261 | 186 |
| Cu | fcc | 3.52 | 3.52 | 3.61 | $a$ | $a$ | $a$ | 189 | 190 | 137 |
| Sr | fcc | 5.73 | | 6.08 | $a$ | $a$ | $a$ | 15 | | 12 |
| Y | hcp | 3.59 | 3.52[b] | 3.65 | 5.35 | 5.61 [b] | 5.73 | 46 | 48 [b] | 37 |
| Zr | hcp | 2.99 | 3.17[b] | 3.23 | 5.57 | 5.14 [b] | 5.15 | 108 | 119 [b] | 83 |
| Nb | bcc | 3.25 | 3.25 | 3.30 | $a$ | $a$ | $a$ | 187 | 193 | 170 |
| Mo | bcc | 3.12 | 3.12[d] | 3.15 | $a$ | $a$ | $a$ | 283 | 291 [d] | 272 |
| Tc | hcp | 2.72 | | 2.74 | 4.34 | | 4.40 | 304 | | 297 |
| Ru | hcp | 2.68 | | 2.71 | 4.26 | | 4.28 | 360 | | 321 |
| Rh | fcc | 3.77 | 3.76 | 3.80 | $a$ | $a$ | $a$ | 306 | 309 | 270 |
| Pd | fcc | 3.85 | 3.85 | 3.89 | $a$ | $a$ | $a$ | 212 | 220 | 181 |
| Ag | fcc | 4.01 | 4.01 | 4.09 | $a$ | $a$ | $a$ | 142 | 142 | 101 |
| Ba | bcc | 4.82 | | 5.02 | $a$ | $a$ | $a$ | 10 | | 10 |
| Hf | hcp | 3.07 | 3.18[b] | 3.19 | 5.08 | 5.15 [b] | 5.05 | 111 | 110 [b] | 109 |
| Ta | bcc | 3.30 | 3.24 | 3.30 | $a$ | $a$ | $a$ | 185 | 224 | 200 |
| W | bcc | 3.14 | 3.14 | 3.16 | $a$ | $a$ | $a$ | 319 | 333 | 323 |
| Re | hcp | 2.78 | 2.77[b] | 2.76 | 4.39 | 4.50 [b] | 4.46 | 371 | 388 [b] | 372 |
| Os | hcp | 2.75 | 2.73[b] | 2.74 | 4.31 | 4.39 [b] | 4.32 | 441 | 440 [b] | 418 |
| Ir | fcc | 3.86 | 3.82[d] | 3.84 | $a$ | $a$ | $a$ | 389 | 401 [d] | 355 |
| Pt | fcc | 3.90 | 3.90 | 3.92 | $a$ | $a$ | $a$ | 318 | 305 | 278 |
| Au | fcc | 4.06 | 4.06 | 4.08 | $a$ | $a$ | $a$ | 187 | 205 | 173 |

[a]First-principles LAPW calculations (Ref. 3).

[b]First-principles APW calculations (Ref. 20).

[c]Nonmagnetic calculation. The experimental structure exhibits some form of magnetism.

[d]First-principles LAPW calculations (Ref. 5).

except tantalum and iridium, and in these cases the discrepancy is less than 2%. Similarly, the equilibrium bulk moduli are in good agreement with the first-principles results, within 10% for all nonmagnetic cubic elements except tantalum, where the error is 17%.

The hexagonal close packed phases were not fit to first-principles results. As a result, the equations of state predicted by the tight-binding model are not as accurate as for the cubic lattices. The largest error is for zirconium, where $a$ is 7% smaller than experiment and $c$ is 8% larger. Yttrium and hafnium also show large discrepancies between the tight-binding model and experiment, and the $c$ for titanium is 2.5% larger than experiment. The lattice constants for the other elements are within 2% of experiment, consistent with the errors we would find in first-principles calculations. We conclude that the tight-binding method is nearly as good as

first-principles LDA methods in determining the structural parameters of hcp metals.

To be successful, the tight-binding method must also show that the experimental ground-state structure is, in fact, the ground state predicted by the method. We have calculated energy versus volume curves for several common crystal structures. As an example, Fig. 4 shows the resulting energy-volume curves for molybdenum. The results for all of the elements are summarized in Table II, which shows the equilibrium energy of each of these phases expressed as the difference in energy between that phase and the equilibrium energy of the experimental ground state. The $c/a$ ratio of the hcp phase has been chosen to minimize the tight-binding energy at each volume to obtain the hcp energies. The tight-binding method correctly predicts the ground-state structure for all metals except the ferromagnetic metals iron and co-

TABLE II. Relative energies per atom of several structures for each of the metals examined by the tight-binding model discussed in the text. The energy of the experimental ground-state structure is arbitrarily set to zero. All energies are calculated at the equilibrium volume found by the tight-binding fit and are expressed in mRy. Below the common name of each phase is its *Strukturbericht* designation.

| | | | | | Structure | | | | | |
|---|---|---|---|---|---|---|---|---|---|---|
| Element | fcc $A1$ | bcc $A2$ | hcp $A3$ | diamond $A4$ | sc $A_h$ | $\alpha$Mn $A12$ | $\beta$Mn $A13$ | $\beta$W $A15$ | AuCu$_3$ $L1_2$ [a] | AlFe$_3$ $D0_3$ [b] |
| Ca | 0.0 | 2.8 | 0.5 | 83.5 | 13.3 | 2.1 | 3.1 | 0.7 | 19.8 | 24.4 |
| Sc | 4.7 | 8.5 | 0.0 | 101.1 | 34.3 | 10.2 | 11.0 | 19.4 | 39.7 | 33.9 |
| Ti | 5.2 | 9.1 | 0.0 | 157.7 | 64.9 | 16.7 | 15.4 | 22.4 | 56.1 | 63.8 |
| V | 19.6 | 0.0 | 19.6 | 180.8 | 76.0 | 11.2 | 12.7 | 12.2 | 62.1 | 53.4 |
| Cr | 28.6 | 0.0 | 30.6 | 49.1 | 118.6 | 20.3 | 19.7 | 16.2 | 94.3 | 87.2 |
| Mn | 7.5 | 14.3 | 2.9 | 44.2 | 90.3 | 0.0 | 1.5 | 7.0 | 87.6 | 66.2 |
| Fe | -27.9 | 0.0 | -35.0 | 79.8 | 54.5 | -23.1 | -25.0 | -8.1 | 4.5 | 20.4 |
| Co | -2.9 | 21.0 | 0.0 | 135.0 | 8.2 | | | 19.2 | 72.7 | 75.2 |
| Ni | 0.0 | 8.0 | 2.8 | 142.3 | 75.9 | 7.7 | 4.6 | 15.0 | 48.7 | 57.1 |
| Cu | 0.0 | 3.5 | 1.2 | 70.8 | 24.7 | 6.2 | 5.4 | 10.1 | 14.7 | 22.0 |
| | | | | | | | | | | |
| Sr | 0.0 | 2.1 | 1.0 | 73.0 | 22.0 | 3.2 | 3.2 | 1.4 | 22.2 | 25.4 |
| Y | 2.4 | 8.8 | 0.0 | 97.9 | 432.2 | 8.6 | 10.4 | 17.3 | 31.5 | 27.5 |
| Zr | 1.1 | 2.9 | 0.0 | 112.7 | 123.3 | 8.6 | 8.0 | 8.0 | 18.7 | 26.2 |
| Nb | 26.1 | 0.0 | 22.7 | 181.9 | 68.6 | 17.1 | 21.1 | 15.9 | 69.5 | 59.6 |
| Mo | 30.0 | 0.0 | 31.0 | 147.3 | 68.7 | 17.5 | 19.9 | 11.3 | 67.7 | 53.5 |
| Tc | 6.1 | 23.3 | 0.0 | 72.9 | 56.3 | 0.2 | 4.5 | 13.3 | 64.6 | 35.4 |
| Ru | 1.0 | 44.6 | 0.0 | 134.5 | 106.6 | 16.3 | 14.6 | 34.7 | 103.0 | 82.7 |
| Rh | 0.0 | 31.7 | 5.1 | 159.8 | 96.0 | 16.3 | 7.4 | 29.5 | 81.2 | 88.3 |
| Pd | 0.0 | 9.9 | 2.5 | 148.6 | 84.9 | 9.2 | 6.1 | 12.8 | 50.1 | 72.8 |
| Ag | 0.0 | 3.3 | 0.6 | 66.1 | 24.1 | 6.0 | 5.3 | 8.6 | 15.7 | 25.2 |
| | | | | | | | | | | |
| Ba | 0.9 | 0.0 | 0.1 | 85.3 | 23.6 | 2.8 | 2.9 | 2.2 | 27.0 | 30.7 |
| Hf | 1.2 | 7.1 | 0.0 | 380.2 | 113 | 22.9 | 20.6 | 20.8 | 110.2 | 143.3 |
| Ta | 24.7 | 0.0 | 25.3 | 188.6 | 63.2 | 8.9 | 14.0 | 9.8 | 65.6 | 54.2 |
| W | 36.0 | 0.0 | 38.2 | 159.3 | 113.7 | 18.2 | 25.7 | 12.4 | 134.2 | 94.2 |
| Re | 13.4 | 27.7 | 0.0 | 28.6 | 55.6 | 0.2 | 1.8 | 19.1 | 61.0 | 22.1 |
| Os | 8.1 | 64.3 | 0.0 | 11.2 | 58.6 | 17.8 | 17.4 | 42.4 | 66.2 | 33.6 |
| Ir | 0.0 | 50.1 | 8.5 | 83.9 | 83.5 | 23.8 | 19.9 | 41.8 | 64.0 | 75.6 |
| Pt | 0.0 | 9.7 | 4.4 | 168.7 | 78.3 | 14.4 | 12.8 | 25.9 | 48.5 | 78.5 |
| Au | 0.0 | 1.4 | 0.6 | 96.1 | 24.1 | 8.7 | 8.4 | 15.2 | 17.5 | 32.3 |

[a]Calculations using the $L1_2$ (AuCu$_3$) lattice, placing the metal atoms on the copper sites and leaving vacancies on the gold sites.

[b]Calculations using the $D0_3$ (AlFe$_3$) lattice, placing the metal atoms on the iron sites and leaving vacancies on the aluminum sites.

balt. This is understandable, since we have not included spin polarization. Especially satisfying is the fact the method finds the correct ground states of the hcp metals and manganese,[26] since these phases are not included in the fit of the tight-binding parameters.

We can also assess the stability of the tight-binding parameters by studying crystal structures of lower symmetry. Thus Fig. 5 shows the energy of molybdenum under a volume-conserving tetragonal strain, the so-called Bain path,[29] at the experimentally observed equilibrium volume of the bcc phase. The energy is properly a minimum for the bcc lattice, where $c/a=1$, and attains a local maximum at the fcc structure ($c/a=\sqrt{2}$), indicating that $C_{11}-C_{12}<0$, so that the fcc structure is unstable. Similarly, Fig. 6 shows the energy

for a monatomic lattice undergoing a trigonal strain with the primitive vectors

$$\begin{pmatrix} \mathbf{a}_1 \\ \mathbf{a}_2 \\ \mathbf{a}_3 \end{pmatrix} = \begin{pmatrix} \alpha & \beta & \beta \\ \beta & \alpha & \beta \\ \beta & \beta & \alpha \end{pmatrix} \begin{pmatrix} \hat{x} \\ \hat{y} \\ \hat{z} \end{pmatrix}, \qquad (12)$$

where $\alpha$ and $\beta$ are chosen so that the volume is the experimentally observed volume of the bcc lattice, and the angle between the primitive vectors is given by $\theta$, where

$$\cos\theta = \frac{(2\alpha+\beta)\beta}{\alpha^2+2\beta^2}. \qquad (13)$$
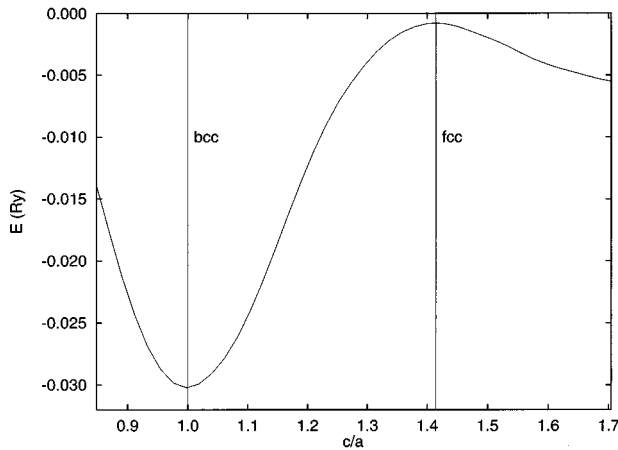
FIG. 5. Tight-binding calculation of the energy of molybdenum, at the experimental equilibrium volume, under a tetragonal strain [the Bain path (Ref. 29)], as a function of $c/a$. The vertical lines denote the positions of the bcc and fcc lattices.

The vectors (12) represent a fcc lattice when $\theta = 60°$, a simple cubic lattice when $\theta = 90°$, and a bcc lattice when $\theta = 109.47°$. The tight-binding calculations in Fig. 6 show that the bcc phase is indeed the minimum-energy structure. Also, the simple cubic phase has a local maximum in the energy, indicating that it is elastically unstable with $C_{44} < 0$.

## IV. ELASTIC CONSTANTS

Elastic constants are calculated by imposing an external strain on the crystal, relaxing any internal parameters to obtain the energy as a function of the strain, and numerically solving for the elastic constants as the curvature of the energy versus strain curve.[2–5] We have calculated the elastic constants for the ground-state phases of all of the elements in this study except manganese. This procedure serves two purposes: it tests the mechanical stability of the proposed tight-binding ground state and it assesses the ability of the method to determine properties not included in the fit of the tight-binding parameters.

The elastic constants of the cubic materials (except manganese) are shown in Table III. This table also shows the elastic constants obtained from first-principles LAPW computations[5] and experiment.[25,30,31] All calculations were performed at the experimental volume. The accuracy of the elastic constants $C_{11}$ and $C_{12}$ is remarkably good. For the 12 elements for which we have first-principles results, none of the tight-binding elastic constants differs from the first-principles results by more than 15%. For comparison, the first-principles results also differ from the experimental results by less than 15%, a measure of the accuracy of the LDA in determining these elastic constants. Thus the tight-binding elastic constants are not significantly worse than those computed from first-principles. Considering only the nonmagnetic materials, the root-mean-square (rms) deviation of the tight-binding $C_{11}$ compared to experiment is 38 GPa, while the rms deviation of $C_{12}$ is 15 GPa.

The errors in $C_{44}$ are somewhat larger, the rms deviation from experiment being 49 GPa. In this case, if we exclude calcium and strontium, discussed below, the maximum deviation of first-principles results from experiment is 22%, in molybdenum. The maximum deviation of the tight-binding elastic constant from the first-principles result is in vanadium, where the error is 114%, even when we use the quadratic Slater-Koster parametrization (11) and split the on-site $d$ terms. As noted above, this is probably due to the high value of the density of states of vanadium near the Fermi level.[19] Excluding vanadium, the maximum deviation is 36%, in niobium. Hence, except for the anomaly of vanadium, the tight-binding results are only slightly worse than the first-principles results in the determination of elastic constants.

Calculation of $C_{44}$ in the alkaline-earth metals is difficult because the lattice is extremely soft. The error in calcium is 71% compared to first-principles results and 50% compared to experiment. For strontium the situation is even worse, since we predict the fcc lattice to be unstable to any strain that is related to $C_{44}$. In this regard, however, it is important to note that even many of the best LDA elastic constant calculations in Table III have an absolute error of more than 10 GPa. Since the experimental values of $C_{44}$ for both calcium and strontium are less than 10 GPa, it is understandable that we cannot reproduce the experimental elastic constants for the alkaline-earth metals with any degree of accuracy.

We also note that this method correctly reproduces the sign of the elastic constant $C_{12} - C_{44}$, even in rhodium and iridium, where it is negative, though the predicted magnitude $|C_{12} - C_{44}|$ is much larger than observed experimentally and in first-principles calculations for these two materials. The negative sign cannot be obtained from the standard embedded-atom method (EAM),[32] though it can be found in the modified embedded-atom method (MEAM).[33]

We have also calculated elastic constants for all of the nonmagnetic transition metals that take the hcp structure. Hexagonal close packed crystals have two atoms per unit cell and the internal parameter describing the atomic positions is free to move when we strain the crystal to calculate elastic constants. Using the tight-binding approach, it is relatively
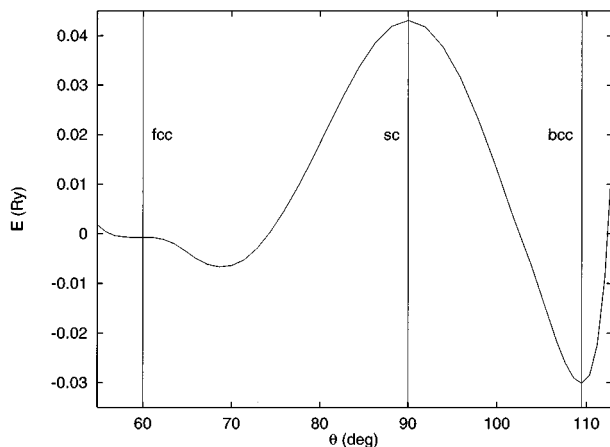


FIG. 6. Tight-binding calculation of the energy of molybdenum, at the experimental equilibrium volume, under a trigonal strain of the lattice given by (12), as a function of the angle between the primitive vectors $\theta$. The positions of the bcc, simple cubic, and fcc lattices are denoted by the vertical lines.

TABLE III. Elastic constants for cubic elements. All elements for which we have constructed a set of tight-binding parameters and which have a cubic ground state (except manganese) are presented here. A comparison is made between the results of our tight-binding parametrization (TB), first-principles full potential LAPW results (LAPW), where available, and experiment (Expt.) (Ref. 25). Where unreferenced, the LAPW results were done for this paper, using previously developed methods (Ref. 4). Calculations were performed at the experimental volume.

| Element | $C_{11}$ TB | LAPW | Expt. | $C_{12}$ TB | LAPW | Expt. | $C_{44}$ TB | LAPW | Expt. |
|---|---|---|---|---|---|---|---|---|---|
| Ca | 15 | 17 [a] | 16 [b] | 10 | 10 [a] | 12 [b] | 4 | 14 [a] | 8 [b] |
| V | 224 | 205 | 228 | 106 | 111 | 119 | 92 | 30 | 43 |
| Cr | 432 | | 346 | 88 | | 66 | 250 | | 100 |
| Fe | -4 | | | 227 | | | 180 | | |
| Ni | 256 | | | 142 | | | 86 | | |
| Cu | 161 | 156 | 168 | 108 | 106 | 121 | 55 | 80 | 75 |
| Sr | 8 | | 15 | 3 | | 6 | -3 | | 10 |
| Nb | 204 | 230 | 246 | 137 | 122 | 139 | 34 | 25 | 29 |
| Mo | 453 | 468 [a] | 450 [c] | 147 | 149 [a] | 173 [c] | 120 | 98 [a] | 125 [c] |
| Rh | 491 | 433 | 413 | 171 | 185 | 194 | 260 | 206 | 184 |
| Pd | 233 | 218 | 227 | 163 | 172 | 176 | 63 | 74 | 72 |
| Ag | 133 | 122 | 124 | 86 | 90 | 93 | 42 | 52 | 46 |
| Ba | 9 | | | 7 | | | 13 | | |
| Ta | 275 | 256 | 261 | 140 | 154 | 157 | 78 | 67 | 82 |
| W | 529 | 527 | 523 | 170 | 194 | 203 | 198 | 147 | 160 |
| Ir | 694 | 621 [a] | 590 | 260 | 256 [a] | 249 | 348 | 260 [a] | 262 |
| Pt | 380 | 381 | 347 | 257 | 189 | 251 | 71 | 83 | 76 |
| Au | 184 | 200 | 189 | 154 | 173 | 159 | 43 | 33 | 42 |

[a]First-principles LAPW calculations (Ref. 5).
[b]Experiment from Ref. 30.
[c]Experiment from Ref. 31.

simple to determine the value of the internal parameter that minimizes the total energy for a given external strain and then find the related elastic constant by standard techniques. This is more difficult for first-principles calculations, so we have not calculated LAPW elastic constants for hexagonal materials. The tight-binding elastic constants are compared to experiment[30] in Table IV. For simplicity in interpreting the results, we calculated the elastic constants using the tight-binding $c/a$ ratio at the experimental volume. The hcp

tight-binding elastic constants show larger relative deviations from experiment than found in the cubic crystals. The largest deviation, 88%, occurs in the calculation of $C_{44}$ in zirconium, where we predict a value of 4 GPa, compared to the 33 GPa found by experiment. The rms deviations of the tight-binding elastic constants from experiment are 46 GPa for $C_{11}$, 17 GPa for $C_{12}$, 25 GPa for $C_{13}$, 54 GPa for $C_{33}$, and 22 GPa for $C_{44}$. The rms deviation over all of the hcp elastic constants is 36 GPa. When compared to the rms deviation for

TABLE IV. Elastic constants for hexagonal close-packed elements. All elements for which we have constructed a set of tight-binding parameters and which have a nonmagnetic hcp ground state are presented here. A comparison is made between the results of our tight-binding parametrization (TB) and experiment (Expt.) (Ref. 30). The tight-binding results include internal relaxation. Calculations were performed at the experimental volume, but at the $c/a$ ratio that minimized the energy for that volume. Note that in a hexagonal crystal, $C_{66} = (C_{11} - C_{12})/2$.

| Element | $C_{11}$ TB | Expt. | $C_{12}$ TB | Expt. | $C_{13}$ TB | Expt. | $C_{33}$ TB | Expt. | $C_{44}$ TB | Expt. |
|---|---|---|---|---|---|---|---|---|---|---|
| Sc | 73 | 99 | 30 | 40 | 31 | 29 | 78 | 107 | 25 | 28 |
| Ti | 171 | 160 | 58 | 90 | 46 | 60 | 203 | 181 | 64 | 47 |
| Y | 45 | 78 | 15 | 29 | 13 | 20 | 48 | 77 | 17 | 24 |
| Zr | 102 | 144 | 67 | 74 | 65 | 67 | 99 | 166 | 4 | 33 |
| Tc | 477 | | 196 | | 172 | 505 | | 127 | | |
| Ru | 642 | 563 | 170 | 188 | 129 | 168 | 706 | 624 | 214 | 181 |
| Re | 559 | 616 | 283 | 273 | 250 | 206 | 621 | 683 | 136 | 161 |
| Os | 754 | | 272 | | 274 | | 831 | | 232 | |

TABLE V. Tight-binding vacancy formation energies compared to first-principles calculations and experiment. Energies were computed using a 108-atom supercell. Calculations with the atoms at the primitive lattice sites in the crystal (Fixed) and allowing relaxation around the vacancy (Relaxed) are shown. First-principles calculations of the vacancy formation energy are given in the column labeled ''LDA.'' The experimental column shows a range of energies if several experiments have been tabulated. Otherwise the estimated error in the experiment is given.

| Element | Vacancy formation energy | | | |
|---|---|---|---|---|
| | Tight-binding | | | |
| | Fixed | Relaxed | LDA | Experiment [a] |
| Cu | 1.29 | 1.18 | 1.41 [b], 1.29 [c] | 1.28 − 1.42 |
| Nb | 2.84 | 2.82 | | 2.65 ± 0.3 |
| Mo | 2.63 | 2.46 | | 3.0 − 3.6 |
| Rh | 3.39 | 3.35 | 2.26 [c] | 1.71 [d] |
| Pd | 2.46 | 2.45 | 1.57 [b] | 1.85 ± 0.25 |
| Ag | 1.31 | 1.24 | 1.20 [b], 1.06 [c] | 1.11 − 1.31 |
| Ta | 3.17 | 2.95 | | 2.9 ± 0.4 |
| W | 6.86 | 6.43 | | 4.6 ± 0.8 |
| Ir | 2.19 | 2.17 | | 1.97 [d] |
| Pt | 2.79 | 2.79 | | 1.35 ± 0.09 |
| Au | 1.24 | 1.12 | | 0.89 ± 0.04 |

[a]Experimental energies as tabulated by Schaefer (Ref. 37), unless otherwise noted.
[b]First-principles calculations of Dederichs et al. (Ref. 35).
[c]First-principles calculations of Polatoglou et al. (Ref. 36).
[d]Experimental energy tabulated by de Boer et al. (Ref. 38).

cubic materials (37 GPa), we see that on average the hcp elastic constants are as accurate as those calculated in the cubic case.

## V. VACANCIES

Vacancy formation energies are most easily determined by the supercell total-energy method.[34] One atom in the supercell is removed and neighboring atoms are allowed to relax around this vacancy while preserving the symmetry of the lattice. The great advantage of the tight-binding method over first-principles calculations is that we can do the calculation in a very large supercell, eliminating the possibility of vacancy-vacancy interactions. We find that a supercell containing 108 atoms is sufficient to eliminate the interaction. The vacancy formation energy is given by

$$E_{\mathrm{vac}}(V) = E_{\mathrm{sc}}(N-1,1;V) - (N-1)E_{\mathrm{bulk}}(V/N), \quad (14)$$

where $E_{\mathrm{sc}}(M,Q;V)$ is the total energy of a supercell of volume $V$ containing $M$ atoms and $Q$ vacancies and $E_{\mathrm{bulk}}(V)$ is the energy per atom of the bulk metal at a volume $V$ per atom. We use the experimental lattice constant to set the volume of the system, since under experimental conditions the lattice constant of a metal containing isolated vacancies will be the lattice constant of the bulk metal.

We have computed the vacancy formation energy of several of the cubic transition and noble metals using this tight-binding method, including relaxation around the vacancy. The results are presented in Table V, where we also compare to first-principles results[35,36] and experiment.[37,38] The calculated vacancy formation energies of niobium, silver, tantalum, and iridium are in excellent agreement with experiment. The tight-binding parametrizations of rhodium, tungsten, and platinum give the poorest vacancy formation energies, 1–2 eV above the experimental value.

We note that the $L1_2$ and $D0_3$ lattices described in Table II can be considered vacancy-containing supercells with $N=4$. Though the vacancy-vacancy interaction in these cells is quite large, fitting the TB parameters [(7)–(10)] to first-principles results for these lattices will improve the vacancy formation energy calculation. We have yet to implement this procedure.

## VI. SURFACES

The tight-binding model can be used to calculate surface energies by the supercell technique. A slab of metal is formed by cleaving the crystal along the desired plane, creating two identical free surfaces. The distance between the two surfaces in increased, creating a set of slabs that repeat periodically in the direction perpendicular to the surfaces. Of course, we must take care to separate the slabs by a large region of vacuum so that the electrons on one slab cannot hop to a neighboring slab. The slabs must be thick enough so that the atoms at the center of the slab have the properties (e.g., local electronic density of states) of atoms in the bulk material and so that the two surfaces on the same slab cannot interact with each other. For low index [(100), (110), and (111)] faces of the nonmagnetic fcc and bcc metals we find that a slab containing 25 atomic layers is sufficient to meet these criteria. We also converge the calculations with respect to the $k$-point mesh. Depending on the surface and underlying bulk structure this takes between 19 and 91 $k$ points in the two-dimensional Brillouin zone. We estimate numerical error in the TB surface energies to be about 0.1 J/m$^2$.

The surface energy, expressed as the energy required to create a unit area of new surface, is then given by the formula

$$E_{\mathrm{surf}} = \frac{1}{2A}(E_{\mathrm{slab}} - NE_{\mathrm{bulk}}), \quad (15)$$

where $A$ is the area occupied by one unit cell on the surface of the slab, $E_{\mathrm{slab}}$ is the total energy of the slab, $N$ is the number of atoms in the unit cell, and $E_{\mathrm{bulk}}$ is the energy of one atom in the bulk at the lattice constant of the atoms in the interior of the slab. For simplicity, the calculations were done using the bulk equilibrium lattice parameters, with no relaxation or reconstruction at the surface. Our calculations indicate that relaxation *energies* are on the order of 1–10 % of the total surface energy, so neglecting relaxation will not significantly alter our conclusions. Of course, relaxation and reconstruction are necessary in order to understand surface properties. We plan to address these issues in the future.

We have calculated the formation energies for bulk terminated (i.e., unrelaxed and unreconstructed), low index [(100), (110), and (111)] surfaces of the nonmagnetic fcc and bcc transition and noble metals. Table VI compares these results to experiment,[39,40] first-principles calculations,[36,41–44] and atomistic models.[33,45,46] Note that, except for the (100) sur-

TABLE VI. Surface energies, calculated from the tight-binding theory (TB), by first-principles local-density methods (LDA), by the embedded-atom method (EAM), or by the modified embedded-atom method (MEAM), compared to experiment. Energies are given in units of $J/m^2$.

| Element | Orientation | TB | LDA | EAM | MEAM [a] | Experiment |
|---|---|---|---|---|---|---|
| V | (111) | 3.34 | | | 1.81 | 2.6 [b] |
| | (110) | 2.13 | | 1.68 [c] | 1.71 | |
| | (100) | 3.04 | | 1.83 [c] | 2.49 | |
| Cu | (111) | 1.73 | 1.94 [d] | 1.17 [e] | 1.41 | 1.77 [f] |
| | (110) | 2.04 | | 1.40 [e] | 1.64 | |
| | (100) | 1.93 | | 1.28 [e] | 1.65 | |
| Nb | (111) | 2.44 | | | 2.02 | 2.3 [b] |
| | (110) | 1.54 | 2.36 [g], 2.9 [h] | 1.81 [c] | 1.87 | |
| | (100) | 2.37 | 2.86 [g], 3.1 [h] | 1.97 [c] | 2.02 | |
| Mo | (111) | 2.84 | | | 1.86 | 2.9 [b] |
| | (110) | 3.04 | 3.14 [g] | 2.13 [c] | 1.93 | |
| | (100) | 2.12 | 3.52 [g] | 2.28 [c] | 2.12 | |
| Rh | (111) | 2.46 | 2.54 [d], 2.53 [g] | | 2.60 | 2.6 [b] |
| | (110) | 2.71 | 2.88 [g] | | 2.92 | |
| | (100) | 2.57 | 2.81 [g] | | 2.90 | |
| Pd | (111) | 1.57 | 1.64 [g] | 1.22 [e] | 1.38 | 2.00 [b] |
| | (110) | 1.86 | 1.97 [g], 2.5 [h], 2.70 [i] | 1.49 [e] | 1.67 | |
| | (100) | 1.75 | 1.86 [g], 2.3 [h], 1.04 [i] | 1.37 [e] | 1.66 | |
| Ag | (111) | 1.14 | 1.21 [g], 1.21 [d] | 0.62 [e] | 1.09 | 1.32 [f] |
| | (110) | 1.42 | 1.26 [g], 1.4 [h] | 0.77 [e] | 1.27 | |
| | (100) | 1.29 | 1.21 [g], 1.3 [h] | 0.71 [e] | 1.22 | |
| Ta | (111) | 3.14 | | | 2.31 | 2.78 [b] |
| | (110) | 2.05 | | 1.80 [c] | 2.17 | |
| | (100) | 3.00 | | 1.99 [c] | 3.29 | |
| W | (111) | 6.75 | | | 2.25 | 2.99 [f] |
| | (110) | 4.30 | | 2.60 [c] | 2.23 | |
| | (100) | 6.7 | 5.54 [j] | 2.81 [c] | 2.65 | 6 [k] |
| Ir | (111) | 2.59 | | | 2.84 | 3.0 [b] |
| | (110) | 3.19 | | | 3.06 | |
| | (100) | 2.95 | | | 2.91 | |
| Pt | (111) | 2.51 | | 1.44 [e] | 1.66 | 2.49 [b] |
| | (110) | 2.97 | | 1.75 [e] | 2.13 | |
| | (100) | 2.83 | | 1.65 [e] | 2.17 | |
| Au | (111) | 1.48 | | 0.79 [e] | 0.89 | 1.54 [f] |
| | (110) | 1.85 | | 0.98 [e] | 1.12 | |
| | (100) | 1.69 | | 0.92 [e] | 1.08 | |

[a]Modified embedded-atom calculations (Ref. 33).

[b]Experimental determination of the surface energy of an ''average'' face using an approximate extrapolation to $T=0$ (Ref. 33).

[c]Embedded-atom calculations for bcc metals (Ref. 46).

[d]Full-potential linearized muffin-tin orbital (full-potential LMTO) calculation, using seven-layer slabs (Ref. 36).

[e]Embedded-atom calculations for fcc metals (Ref. 45).

[f]Experimental determination of the surface energy of an average face at $T=0$ (Ref. 39).

[g]FP LMTO calculation, using seven-layer slabs (Ref. 42).

[h]Full-Potential LAPW calculation, using nine-layer slabs (Ref. 43).

[i]Local orbital pseudo-potential calculation, using a three-layer slab. (Ref. 41).

[j]Full-potential linearized augmented plane-wave (LAPW) calculation for the ideal surface, using a five-layer slab (Ref. 44).

[k]Experimental result for the (100) surface (Ref. 40).

face of tungsten, the experimental results[33,39] are for an ''average'' surface and some are extrapolated to $T=0$ from high temperatures.[33]

The results for the fcc metals are particularly gratifying. In all cases we find $E_{(111)}<E_{(100)}<E_{(110)}$. Thus close packed surfaces are the most stable for the fcc metals. The TB surface energies are uniformly larger, and closer to experiment, than those obtained by the EAM,[45] which is known to underestimate surface energies in fcc metals. Our surface energies are generally closer to experiment than those obtained by the MEAM (Ref. 33) and in good agreement with first-principles calculations of the surface energy of copper(111) (Ref. 36) and rhodium.[42] Our calculations are also in the range of the surface energies predicted by several first-principles calculations for palladium and silver.[41–43]

Results for bcc metals are also good. For all of the unrelaxed surfaces we find $E_{(110)}<E_{(100)}<E_{(111)}$. The energies for niobium and molybdenum are somewhat low compared to both first-principles calculations[42,43] and experiment, but the only serious discrepancy is the average surface energy of tungsten, which is smaller than our values by a factor of one-third. At the moment this is not particularly worrisome, because experimental estimates of the surface energy of tungsten range from 1.68 J/m$^2$ to 4.50 J/m$^2$.[47] The latter number is, in fact, in range of our calculation for the (110) surface. In addition, the results for the energy of the (100) surface of tungsten are in good agreement with both first-principles results[44] and experiment.[40] In most cases the tight-binding surface energies are greater than either of the corresponding EAM or MEAM values. Where this is not the case the energy difference is slight.

## VII. SUMMARY

We have extended the tight-binding method[1] to include most of the alkaline-earth, transition, and noble metals. Tight-binding parameters are determined by doing a least-squares fit to simultaneously reproduce the total energy and electronic structure determined by first-principles at several volumes of the fcc and bcc lattices. In all cases except the ferromagnetic metals the method correctly predicts the ground-state structure, even when the ground state is hcp or $\alpha$Mn.

The method was tested against first-principles results and experiment by the calculation of elastic constants, vacancy formation energies, and surface energies. Elastic constants for nonmagnetic cubic materials are, in general, in good agreement with both LAPW calculations and experiment, though we have some problems with $C_{44}$ in vanadium. Since the tight-binding method does not require a specific sign for $C_{12}-C_{44}$ we get reasonable elastic constants even for rhodium and iridium. Elastic constants for the hcp phase are nearly as accurate as those calculated in the cubic phase.

Compared to experiment, the accuracy of the vacancy formation energy predictions range from good to poor, with niobium, silver, tantalum, and iridium all in excellent agreement with experiment and rhodium, tungsten, and platinum much larger than experiment. Surface energies for both fcc and bcc crystals are in good agreement with the available first-principles and experimental data. Energies for fcc crystals are uniformly larger than the corresponding EAM energies, in agreement with experiment.

Improvements to the tight-binding method are under investigation. In particular, we are examining other forms for the parametrization of the on-site terms (9) and the Slater-Koster terms (10). We are also investigating the effect of two-center Slater-Koster integrals on the on-site terms, as suggested by Mercer and Chou.[18] Since these terms properly account for the crystal-field splitting of the on-site terms, they may be useful in obtaining even more accurate results. Finally, we have begun the process of extending the tight-binding method to binary systems.[48]

## APPENDIX:  TIGHT-BINDING PARAMETERS

The tight-binding parameters used in this paper are available from the AIP Physics Auxiliary Publication Service, http://www.aip.org/epaps/epaps.html, as noted in a footnote to this paper,[49] on the World Wide Web at http://cst-www.nrl.navy.mil/bind,     or     via     email     at mehl@dave.nrl.navy.mil

[1] R. E. Cohen, M. J. Mehl, and D. A. Papaconstantopoulos, Phys. Rev. B **50**, 14 694 (1994).

[2] M. J. Mehl, J. E. Osburn, D. A. Papaconstantopoulos, and B. M. Klein, Phys. Rev. B **41**, 10 311 (1990); **42**, 5362(E) (1991).

[3] M. J. Mehl, J. E. Osburn, D. A. Papaconstantopoulos, and B. M. Klein, in *Alloy Phase Stability and Design*, edited by G. M. Stocks, D. P. Pope, and A. F. Giamei, MRS Symposia Proceedings No. 186 (Materials Research Society, Pittsburgh, 1991), p. 227.

[4] M. J. Mehl, Phys. Rev. B **47**, 2493 (1993).

[5] M. J. Mehl, B. M. Klein, and D. A. Papaconstantopoulos, in *Intermetallic Compounds: Principles and Applications*, edited by J. H. Westbrook and R. L. Fleischer (Wiley, London, 1994), Vol. 1.

[6] P. Hohenberg and W. Kohn, Phys. Rev. **136**, B864 (1964).

[7] W. Kohn and L. J. Sham, Phys. Rev. **140**, A1133 (1965).

[8] M. J. Gillan, J. Phys. Condens. Matter **1**, 689 (1989).

[9] M. M. Sigalas and D. A. Papaconstantopoulos, Phys. Rev. B **49**, 1574 (1994).

[10] C. H. Xu, C. Z. Wang, C. T. Chan, and K. M. Ho, J. Phys. Condens. Matter **4**, 6047 (1992).

[11] L. Goodwin, A. J. Skinner, and D. G. Pettifor, Europhys. Lett. **9**, 701 (1989).

[12] A. E. Carlsson, Phys. Rev. B **44**, 6590 (1991).

[13] A. P. Sutton, M. W. Finnis, D. G. Pettifor, and Y. Ohta, J. Phys. C **21**, 35 (1988).

[14] J. L. Mercer, Jr. and M. Y. Chou, Phys. Rev. B **47**, 9366 (1993).

[15] M. Menon, J. Connolly, N. Lathiotakis, and A. Andriotis, Phys. Rev. B **50**, 8903 (1994).

[16] N. N. Lathiotakis, A. N. Andriotis, M. Menon, and J. Connolly, Europhys. Lett. **29**, 135 (1995).

[17] J. C. Slater and G. F. Koster, Phys. Rev. **94**, 1498 (1954).

[18] J. L. Mercer, Jr. and M. Y. Chou, Phys. Rev. B **49**, 8506 (1994).

[19] D. A. Papaconstantopoulos, *Handbook of Electronic Structure of Elemental Solids* (Plenum, New York, 1986).

[20] M. Sigalas, D. A. Papaconstantopoulos, and N. C. Bacalis, Phys. Rev. B **45**, 5777 (1992); *ibid.* M. M. Sigalas and D. A. Papaconstantopoulos, **50**, 7255 (1994).

[21] O. K. Andersen, Phys. Rev. B **12**, 3060 (1975).

[22] S. H. Wei and H. Krakauer, Phys. Rev. Lett. **55**, 1200 (1985).

[23] L. Hedin and B. I. Lundqvist, J. Phys. C **4**, 2064 (1971).

[24] J. J. More, in *Numerical Analysis*, edited by G. A. Watson (Springer-Verlag, Berlin, 1977).

[25] G. Simmons and H. Wang, *Single Crystal Elastic Constants and Calculated Aggregate Properties: A Handbook*, 2nd ed. (MIT Press, Cambridge, MA, 1971).

[26] M. J. Mehl and D. A. Papaconstantopoulos, Europhys. Lett. **31**, 537 (1995).

[27] C. Kittel, *Introduction to Solid State Physics* (Wiley, New York, 1971).

[28] J. Donohue, *The Structures of the Elements* (Wiley, New York, 1974), pp. 191–199.

[29] E. C. Bain, Trans. AIME **70**, 25 (1924).

[30] *Smithells Metals Reference Book*, 6th ed., edited by E. A. Brandes (Butterworths, London, 1983).

[31] F. H. Featherstone and J. R. Neighbors, Phys. Rev. **130**, 1324 (1963).

[32] A. F. Voter, in *Intermetallic Compounds: Principles and Applications* (Ref. 5), Vol. 1.

[33] M. I. Baskes, Phys. Rev. B **46**, 2727 (1992).

[34] M. J. Mehl and B. M. Klein, Physica B **172**, 211 (1991).

[35] P. H. Dederichs, T. Hoshino, B. Drittler, K. Abraham, and R. Zeller, Physica B **172**, 203 (1991).

[36] H. M. Polatoglou, M. Methfessel, and M. Scheffler, Phys. Rev. B **48**, 1877 (1993).

[37] H.-E. Schaefer, Phys. Status Solidi A **102**, 47 (1987).

[38] F. R. de Boer, R. Boom, W. C. M. Mattens, A. R. Miedema, and A. K. Niessen, *Cohesion in Metals* (North-Holland, Amsterdam, 1988), Vol. 1.

[39] W. R. Tyson and W. A. Miller, Surf. Sci. **62**, 267 (1977).

[40] E. Cordwell and D. Hull, Philos. Mag. **19**, 951 (1969).

[41] D. Tománek, Z. Sun, and S. G. Louie, Phys. Rev. B **43**, 4699 (1991).

[42] M. Methfessel, D. Hennig, and M. Scheffler, Phys. Rev. B **46**, 4816 (1992).

[43] M. Weinert, R. E. Watson, J. W. Davenport, and G. W. Fernando, Phys. Rev. B **39**, 12 585 (1989).

[44] D. Singh, S.-H. Wei, and H. Krakauer, Phys. Rev. Lett. **57**, 3292 (1986).

[45] S. M. Foiles, M. I. Baskes, and M. S. Daw, Phys. Rev. B **33**, 7983 (1986).

[46] A. M. Guellil and J. B. Adams, J. Mater. Res. **7**, 639 (1992).

[47] W. R. Tyson, Can. Metall. Q. **14**, 307 (1975).

[48] D. A. Papaconstantopoulos and M. J. Mehl, in *Materials Theory, Simulations, and Parallel Algorithms*, edited by E. Kaxiras, J. Joannopoulos, P. Vashishta, and R. K. Kalia, MRS Symposia Proceedings No. 408 (Materials Research Society, Pittsburgh, 1996), p. 31.

[49] See AIP Document No. E-PRBMD-54-4519-215kb 29 tight-binding parameter files, a README file, and the Latex version of this paper (a total of 215 KB). The files are available for retrieval via FTP either over the WWW from http://www.aip.org/epaps/epaps.html or via anonymous FTP from ftp.aip.org in the directory /epaps/. There is no charge associated with retrieving these files.